Materials and Design 111 (2016) 44–50

Contents lists available at ScienceDirect

Materials and Design

journal homepage: www.elsevier.com/locate/matdes

3-Dimensional hierarchical porous activated carbon derived from coconut fibers with high-rate performance for symmetric supercapacitors

Lihong Yin, Yong Chen *, De Li, Xiaoqin Zhao, Bo Hou, Bokai Cao

Laboratory of Tropic Biological Resources, MOE, Hainan Provincial Key Laboratory of Research on Utilization of Si-Zr-Ti Resources, Hainan University, 58 Renmin Road, Haikou 570228, China

HIGHLIGHTS

- Coconut fibers with multi-tubular hollow structure were used to prepare activated carbon by carbonization and activation.
- Multi-tubular hollow structures were maintained and micro/mesopores were created on the wall.
- Special structures could shorten the diffusion paths resulting in high-rate performance.

GRAPHICAL ABSTRACT

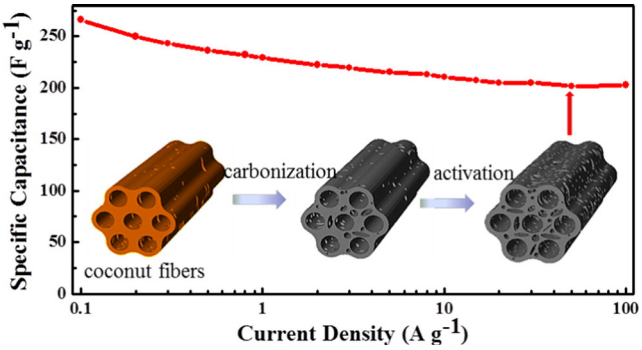

ARTICLE INFO

Article history:
Received 8 June 2016
Received in revised form 22 August 2016
Accepted 24 August 2016
Available online 26 August 2016

Keywords:
Coconut fibers
3-Dimensional hierarchical porous activated carbon
High energy density
High rate performance
Symmetric supercapacitors

ABSTRACT

Here we report a 3-dimensional hierarchical porous activated carbon (HPAC) prepared from coconut fibers with KOH activation, which exhibits high-rate performance for symmetric supercapacitors. At a 4:1 mass ratio of KOH to carbonized coconut fibers, the highest specific surface area of 2898 $m^2 g^{-1}$ with a pore volume of 1.59 $cm^3 g^{-1}$ (30% mesopores) is successfully achieved in a 3-dimensional HPAC. As a supercapacitor electrode combined with a 6 M KOH electrolyte, a high specific capacitance of 266 F g^{-1} at a current of 0.1 A g^{-1} is successfully achieved and an excellent rate performance up to 76% of its capacitance is retained at a high current of 100 A g^{-1}. Additionally, in $EMIMBF_4$ electrolyte, 3-dimensional HPAC electrode exhibit a high capacitance of 155 F g^{-1} at 0.1 A g^{-1} and 142 F g^{-1} at 10 A g^{-1}. Owing to its excellent rate performance, 3-dimensional HPAC can deliver a high energy density of 53 Wh kg^{-1} and a high power density of 8224 W kg^{-1}, which shows promising application potential in energy storage devices.

1. Introduction

Energy advancement promotes the development of our society, yet challenges still exist in the storage and delivery of energy. In these decades, people are trying to substitute sustainable technologies for conventional fossil fuel-based solutions by seeking renewable, low-cost and abundant energy resources, as well as developing new technologies of energy conversion and storage [1–4]. Rechargeable batteries are considered to be a promising solution for sustainable energy technologies, while their disadvantages of short cycle life (1000 cycles) and low power density prevent them from meeting the increasing demands

* Corresponding author.
E-mail address: ychen2002@163.com (Y. Chen).

http://dx.doi.org/10.1016/j.matdes.2016.08.070
0264-1275/

of renewable technologies such as electrical vehicles [2]. Electrochemical supercapacitors, another example of an energy storage and conversion system, have become increasingly popular due to their high power density, excellent cycle stability, and compromise of the power/energy between traditional dielectric capacitors and batteries [1,5]. However, for some power applications, supercapacitors are mostly confined to a low energy density (<10 Wh kg^{-1}) in comparison with lithium-ion batteries (160 Wh kg^{-1}) [6,7].

Currently, activated carbon has been commercially utilized as an electrode material for supercapacitors, owing to their low cost versus other porous carbons (e.g. templated carbons and carbide derived carbons) [8]. For carbon-based electrical double layer capacitors (EDLCs), specific surface area, pore size distribution and structure, and electrical conductivity are critical parameters for the device's performance [9]. In certain cases, activated carbons with large micropore surface area only exhibit a finite growth of electric double-layer capacitance, ascribing to a tortuous path for electrolyte ions to access the inner pore surface area [10–12]. In addition, the restriction on diffusion velocity also makes the specific capacitance descend rapidly at high current densities [13,14]. Therefore, to enhance capacitance performance, it should be designed of high specific surface area activated carbons with the interconnected pores and short pore length, in which the amount of mesopores are critical to accelerate ion transport and raise the accessible surface area [14–18].

Compared with other synthetic routes, fabricating hierarchical porous carbon from natural plant and biomass waste has the advantages of high-yield, low-cost and less pollution [19]. Coconut generally grows in tropical and sub-tropical regions and produces a large quantity of coconut shell fibers although the year, yet only a small part is used for ropes, brushes, palm mattresses, etc. In this study, a simple and economic strategy is adopted to prepare hierarchical porous carbon by traditional KOH activation of carbonized coconut fibers. The experimental results prove that the coconut shell fibers, with a distinctive multitubular hollow structure, are a suitable raw material for preparing 3-dimensional hierarchical porous activated carbon (HPAC) possessing high specific surface area. As an electrode material for supercapacitors, the 3-dimensional HPAC delivers a large energy density and high rate performance. Hence, the coconut shell fibers could be adopted as a readily available, renewable and cost-effective raw material for supercapacitor electrodes possessing excellent electrochemical properties.

2. Experimental section

2.1. Material synthesis

A typical preparation procedure consists of two steps. First, the ground coconut fibers (CF, Haikou, China) were carbonized by heating with a rate of 3 °C min^{-1} to 700 °C and maintaining this temperature for 1 h under a nitrogen atmosphere. Second, the CF carbonized materials (referred to as CFC) were mixed at different ratios of KOH (Guangzhou Chemical Reagent Corp. China) and activated by heating at a rate of 3 °C min^{-1} to 850 °C and maintaining this temperature for 1 h under a nitrogen atmosphere, followed by washing with dilute HCl solution (2%, Shanghai Chemical Reagent Co., Ltd., China) and then deionized water until pH ≈ 7. Finally, the samples were dried at 120 °C for 12 h. The resultant samples were denoted as HPAC-X, where X represents the mass ratio of KOH to CFC. The preparation process can be illustrated by the following schematic of Fig. 1.

2.2. Characterization methods

N_2 (77 K) adsorption/desorption (JW-BK122W, Beijing JWGB Sci. & Tech. Co., China) were used to measure the specific surface area and the porosity of CFC and HPAC, and the Brunauer-Emmett-Teller (BET) method and non-localized density function theory (NLDFT) were implemented to calculate the specific surface area and pore size distribution, respectively, in which all samples were degassed in vacuum at 120 °C for 4 h before measurements. The morphology and microstructure were characterized via field emission scanning electron microscopy (SEM, Hitachi S-4800, Japan), transmission electron microscopy (TEM, JEM-2100, JEOL, Japan) at an operating voltage of 200 kV.

2.3. Electrochemical measurements

A symmetrical two-electrode cell was used to measure the electrochemical performance of HPAC, as shown in Fig. 2. Briefly, the as-prepared samples were mixed with Ketjen black (Lion Corp., Japan) and polytetrafluorethylene (PTFE, 60% dispersion in water, Sigma-Aldrich, USA) at a mass ratio of 80:15:5 to form a paste, which was pressed into a film with a roller and cut into 10 mm diameter pieces. Then the pieces were pressed on the current collector (12 mm in diameter) at a pressure of 10 MPa (30 s), and then dried at 110 °C for 6 h in

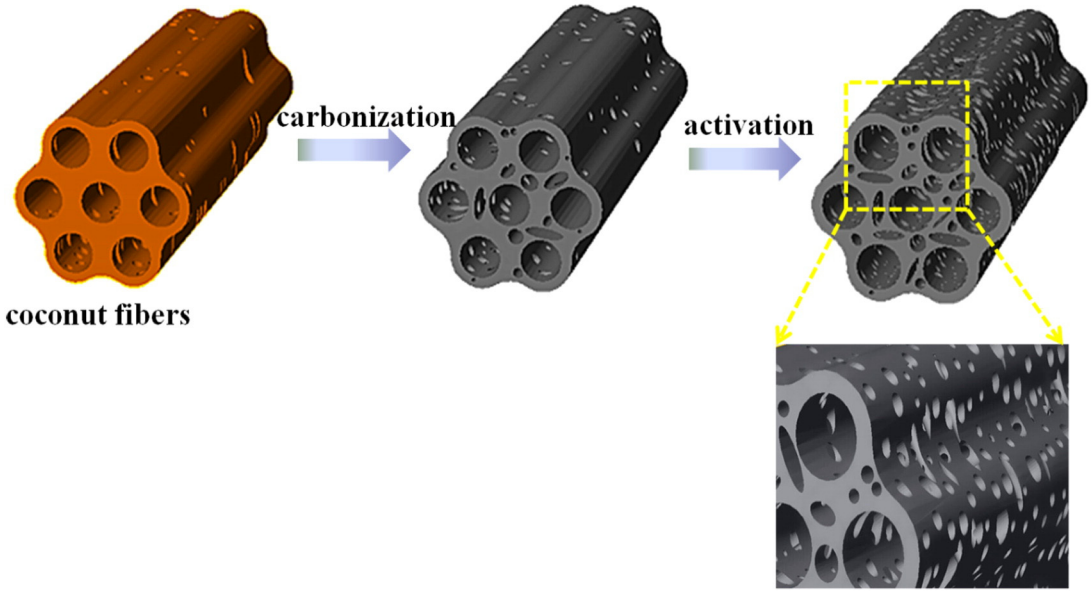

Fig. 1. Schematic illustration of the synthesis of 3-dimensional HPAC from coconut fibers.

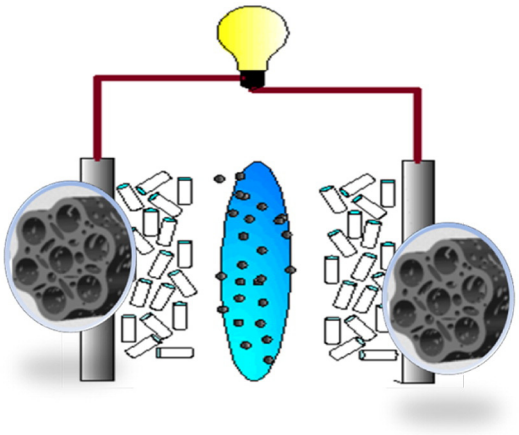

Fig. 2. Schematic of symmetric supercapacitor with 3-dimensional HPAC electrodes.

sequence. The electrodes/collectors were assembled in CR2025 stainless steel coin cells (Shenzhen Teensky Ltd., China) with the separator of glass fibers (GF/A Whatman, UK) and the electrolyte of 6 M KOH aqueous solution or 1-ethyl-3-methylimidazolium tetrafluoroborate ($EMIMBF_4$, for electrochemistry ≥99.0%, Sigma-Aldrich, USA). The active material on each electrode was approximately 1.0–2.0 mg.

Cyclic voltammetry (CV) and electrochemical impedance spectroscopy (EIS) were conducted on an Electrochemical Workstation (VSP300, Bio-logic, France). The CV measurements were carried out in 6 M KOH and $EMIMBF_4$ in the range of 0–1.0 V and 0–3.5 V, respectively. The EIS was performed at an open circuit potential over a frequency range from 100 kHz to 10 MHz at an amplitude of 5 mV. Galvanostatic charge/discharge (GCD) was conducted by the LAND CT2001 (LAND, China) testing instrument at an identical voltage range as the CV measurements.

The specific capacitance values of a single electrode were calculated according to Eq. (1):

$$C_s = \frac{2 \times I_{cons} \times \Delta t}{m \times \Delta V} \tag{1}$$

where I_{cons} (A) is the discharge current, m is the mass of active material on one electrode, Δt (s) is the discharge time, and ΔV (V) is the voltage change during discharge (excluding the IR drop).

The energy density (E, Wh kg^{-1}) and power density (P, W Kg^{-1}) of the cells were calculated according to Eqs. (2) and (3):

$$E = \frac{C_s \times V_{max}^2}{2 \times 4 \times 3.6} \tag{2}$$

where V_{max} is the cell voltage after IR drop.

$$P = \frac{E \times 3600}{\Delta t} \tag{3}$$

3. Results and discussion

As stated in literature, coconut fibers possess natural multi-tubular hollow structure with closely distributed pores on the walls, which can be utilized to synthesize the active carbon. The porous fibers possess a number of capillaries with strong absorbability, allowing KOH active agent to easily access and uniformly distribute to the interior of the coconut fibers, which is imperative for obtaining homogenous porous materials [20]. After activation, the retained unique structure can shorten the transport distance and minimize the diffusion resistance of electrolyte species, which is significant to improve of electrochemical properties.

The structure and morphology of coconut fibers and the as-synthesis 3-dimensional HPAC were characterized via SEM and TEM. The pristine material consists of numerous bundles of coconut fibers with natural pores on the walls, as shown in Fig. 3a. During the carbonization, biopolymers are pyrolyzed to form a carbon framework. After that, the hollow fiber structures are still maintained, according to their cross section in Fig. 3b, to provide large surface area for KOH. In Fig. 3c, the tubular structures of the HPAC-4 are preserved and the channels can be seen clearly. It should also be noted that the TEM image (Fig. 3d) of HPAC-4 reveals a structure consisting of amorphous carbon.

To further examine the porous structure of CFC and HPAC-X, N_2 adsorption-desorption isothermal analysis was adopted. The isotherms of CFC and HPAC-1, 2 exhibit a typical I-type curve with a sharp nitrogen adsorption taking place at a relative pressure below 0.1, indicative of a typical microporous structure (Fig. 4a) [21]. Results reveal that CFC has a relatively low specific surface area of 33 $m^2\ g^{-1}$ and a pore volume of 0.08 $cm^3\ g^{-1}$ after 700 °C carbonization. After KOH activation, both the specific surface area and pore volume are significantly increased at a weight ratio of KOH/CFC when increased from 1 to 4 then decreased when the ratio increased to 5. In addition, the knee in the isotherm becomes wider, suggesting the generation of mesopores and the broadening of pore size distributions [22]. Moreover, the pore size distributions (PSDs) by NLDFT model (Fig. 4b) reveals that the pore volume is rapidly increased in comparison with CFC, and the pore size increases during the activation with an increase of the ratio of KOH/CFC. Therefore, the larger the weight ratio of KOH/CFC (while still below 5), the larger the size of both micropores and mesopores as well as the volume of mesopores. As shown in Table 1, a maximum specific surface area of 2898 $m^2\ g^{-1}$ and pore volume 1.59 $cm^3\ g^{-1}$ with mesoporous volume up to 30% was achieved with a KOH/CFC ratio of 4. The average pore diameter of HPAC-4 was determined to be 2.2 nm and the micropore and mesopore diameters are primarily in the range of 0.8 and 2.8 nm, respectively.

In combination with N_2 adsorption results and SEM/TEM images, it can be seen that the HPAC contains macropores, mesopores and a substantial amount of micropores that create an interconnected structure on the wall of the tube. For energy storage applications, the channel of hollow fibers can act as ion-buffering reservoirs that can shorten diffusion distance from the external electrolyte to the interior surface, the mesopores of the walls provide low-resistant pathways for the ions through the porous particles, and the micropores strengthen the electric-double-layer capacitance. Therefore, the HPAC utilized as an electrode for EDLCs are expected to exhibit excellent capacitive performance especially during high charge-discharge rates.

In order to evaluate the performance of the HPAC-X, electrochemical measurements were tested on coin cells with 6 M KOH aqueous solution as the electrolyte. All CV curves retain quasi-rectangular shape recorded at 200 mV s^{-1}, indicating ideal capacitive behavior (Fig. 5a). Additionally, HPAC-4 demonstrates the largest area under the CV curve that indicates the highest specific capacitance. As shown by the galvanostatic charge-discharge (GCD) curves (Fig. 5b), HPAC can be easily charged and discharged with symmetric and well-defined charge-discharge lines at 1 A g^{-1}, demonstrating excellent electrochemical stability and reversibility. Thus, HPAC-4 possesses the highest capacitance in agreement with CV measurements. The specific capacitance values of HPAC-1, HPAC-2, HPAC-3, HPAC-4, and HPAC-5 that are calculated from GCD curves at 1 A g^{-1} are 133 F g^{-1}, 159 F g^{-1}, 203 F g^{-1}, 228 F g^{-1}, and 201 F g^{-1}, respectively. The Nyquist plots (Fig. 5c) further depict that the HPAC exhibits vertical curves at low frequencies, indicative of an ideal capacitive behavior. In comparison to others, at high frequencies the HPAC-4 shows a lower equivalent series resistance (ESR) and shorter Warburg region portion on account of the better electrical conductivity as well as enhanced ion transmission. In order to further investigate the high rate performance, specific capacitance is tested under varying current densities (Fig. 5d). HPAC-4's specific capacitance can reach 266 F g^{-1} at 0.1 A g^{-1}, and retain 76%, i.e. 202 F g^{-1} at a

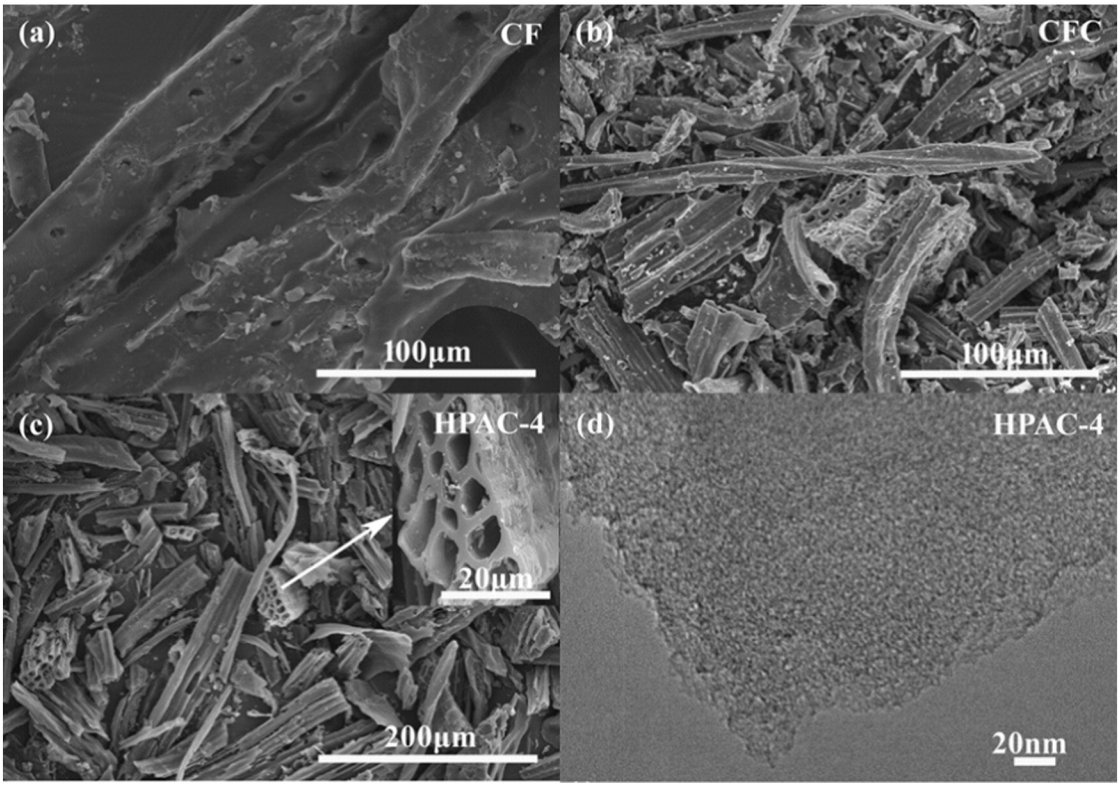

Fig. 3. SEM images of CF (a), CFC (b) and HPAC-4 (c), and TEM image of HPAC-4 (d).

density of 100 A g^{-1}. In order to clearly elucidate the high rate performance of the as-prepared HPAC-4, comparisons were performed with some reported representative carbon-based materials, such as hierarchically porous graphitic carbon fibers derived from cotton (61% capacitance retention from 1 to 60 A g^{-1}) [19], microporous carbon nanofibers prepared by electrospinning from resole-type phenolic resin (a retention of 67% from 0.2 A g^{-1} to 20 A g^{-1}) [23], and bio-inspired beehive-like hierarchical nanoporous carbon derived from bamboo-based industrial byproduct (63.8% capacitance retention over a wide range of current densities from 0.1 to 100 A g^{-1}) [24]. In addition, the CV cures of HPAC-4 over a wide range of scan rates were also investigated (Fig. 5e), in which the results verify that the rectangular shape signifying typical capacitive behavior is maintained even at 500 mV s^{-1}, potentially due to fast and efficient charge response within the unique structure. The HPAC-X also displayed good stability after 10,000 cycles at 1 A g^{-1} and HPAC-4 displays the more superior stability with 84% capacitance retention (Fig. 5f). According to the above tests, among HPAC-X, HPAC-4 possesses higher efficient specific surface area resulting in larger capacitance and more appropriate pore size distribution simultaneously facilitating ion transport by providing a smaller resistance, demonstrating that the HPAC-4 is more promising material as advanced electrodes for electrochemical supercapacitors.

Another study was conducted for exploring a higher energy density with $EMIMBF_4$ as the electrolyte which can charge to 3.5 V. The typical rectangular CV curve from 0 to 3.5 V was obtained up to 200 mV s^{-1} (Fig. 6a). This behavior ascribed to the enlarged size pores in the HPAC-4, indicative of facile ion diffusion within the multi-tubular hollow structure. The GCD curves of the HPAC-4 are highly symmetrical and display nearly linear slopes along with a rather limited voltage drop even if up to 10 A g^{-1}, yielding a high gravimetric capacitance at 0.1 A g^{-1} as well as 10 A g^{-1}, up to 155 F g^{-1}, 142 F g^{-1}, respectively (Fig. 6b, c). Here, excellent high-rate performance of the assembled supercapacitor should be attributed to its unique multi-tubular hollow structure and an optimum pore size distribution. Furthermore, from

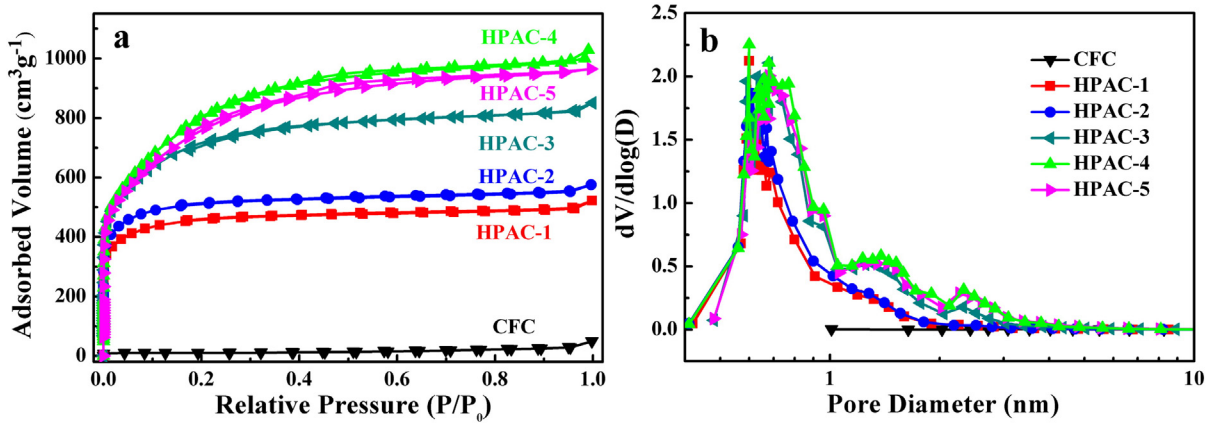

Fig. 4. Nitrogen adsorption/desorption isotherms (a) and the NLDFT pore-size distribution curves (b) of CFC and different HPAC.

Table 1
List of parameters deduced from nitrogen adsorption/desorption analysis for different materials.

Sample	S_{BET} ($m^2\ g^{-1}$)	S_{mic} ($m^2\ g^{-1}$)	S_{meso} ($m^2\ g^{-1}$)	V_t ($cm^3\ g^{-1}$)	V_{mic} ($cm^3\ g^{-1}$)	V_{meso} ($cm^3\ g^{-1}$)
CFC	33	7	26	0.08	0.02	0.06
HPAC-1	1734	1608	126	0.81	0.68	0.13
HPAC-2	1966	1825	141	0.89	0.76	0.13
HPAC-3	2495	2038	457	1.32	1.05	0.27
HPAC-4	2898	1937	961	1.59	1.11	0.48
HPAC-5	2589	1590	999	1.49	1.08	0.41

S_{BET}: specific surface area; S_{mic}: micropore surface area; S_{meso}: mesopore surface area; V_t: total pore volume; V_{mic}: micropore volume; V_{meso}: mesopore volume.

the EIS results in Fig. 6d, it can be seen that the ESR is relatively low while the Warburg region is shorter. Typically, the energy density will decrease as the power density increases [25–29], but the devices prepared herein demonstrate a relatively stable performance as power density increases at a high charge-discharge rate. At 0.1 A g^{-1}, the energy density can reach 66 Wh kg^{-1} as shown in the Ragone plot for HPAC-4 based symmetrical supercapacitor (Fig. 6e), demonstrating much higher results than commercial devices (i.e., EDLCs < 8 Wh kg^{-1}, pseudocapacitors < 30 Wh kg^{-1}) [30,31], a hybrid supercapacitor (55 Wh kg^{-1}) [32]. Moreover, up to 10 A g^{-1}, the energy density can be maintained at 53 Wh kg^{-1} with a power density of 8224 W kg^{-1}. Relative to the rice bran [33], HPAC-4 maintains a higher energy density with a high power density highlighting its excellent rate performance and its enhancement from other activated carbons like carton box [34] and human hair [35] with testing in organic electrolyte (Fig. 6e). The cyclic stability test over 10,000 cycles at 0.5 A g^{-1} demonstrates excellent stability of HPAC-4 with 81% retention rate (Fig. 6f).

The outstanding performance shown by HPAC-based supercapacitors, such as high specific capacitance as well as excellent rate capacity, can be attributed to the following factors: (1) the intrinsic multi-tubular hollow structure in HPAC facilitates fast ion diffusion and interconnected pores that provide a continuous pathway for electron transport; (2) an ultrahigh specific surface, 2898 $m^2\ g^{-1}$ of HPAC-4,

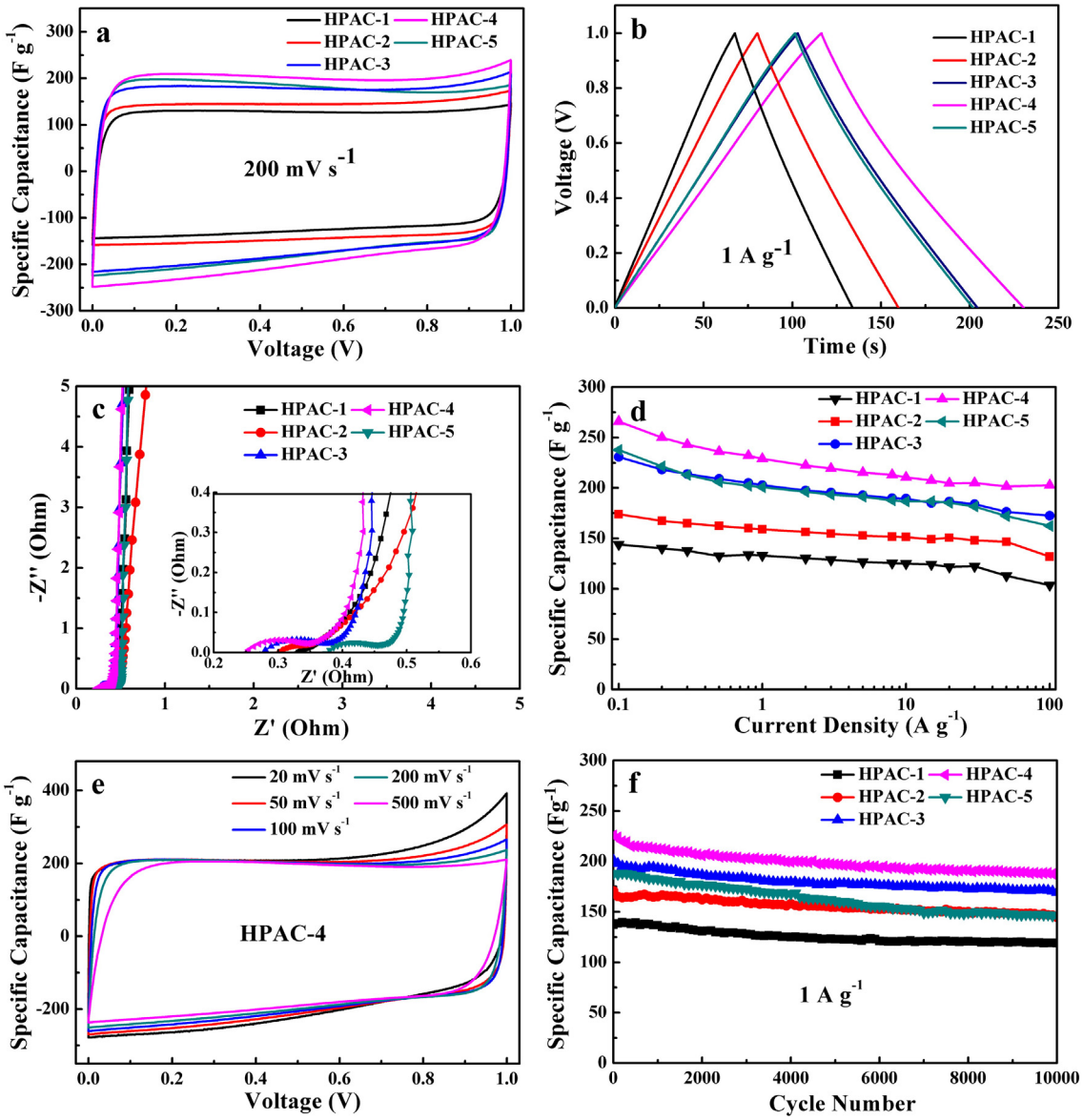

Fig. 5. Electrochemical performance of HPAC in a two-electrode system with 6 M KOH electrolyte. (a) CV curves at a scan rate of 200 mV s^{-1}; (b) Galvanostatic charge/discharge curves at a current density of 1 A g^{-1}; (c) Nyquist plots of EIS spectra; (d) Specific capacitance at varying current densities; (e) CV curves of HPAC-4 at varying scan rates; (f) Cycling stability at 1 A g^{-1}.

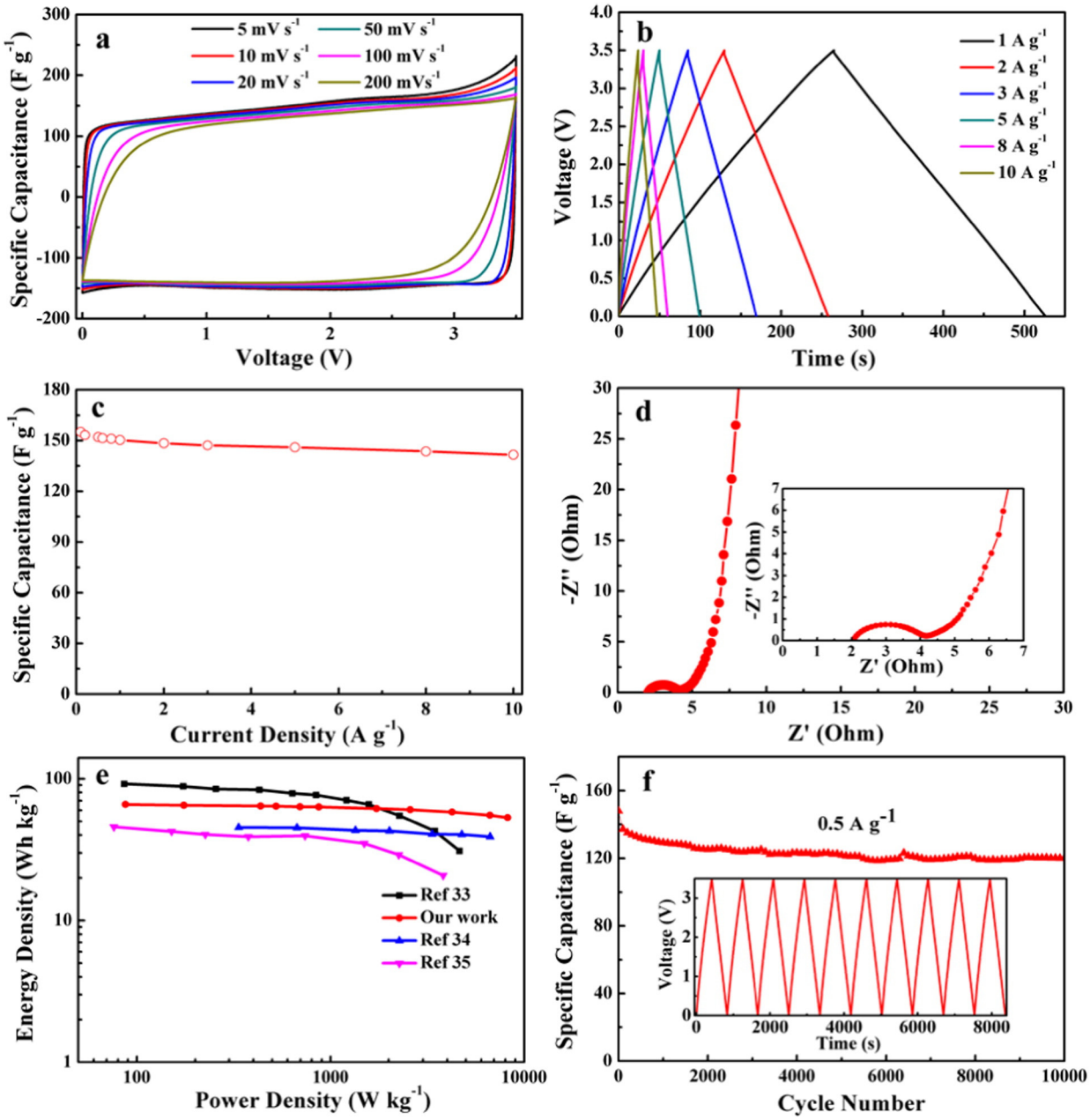

Fig. 6. Electrochemical performance of HPAC-4 in a two-electrode system with $EMIMBF_4$. (a) CV curves at various scan rates; (b) galvanostatic charge/discharge curves at various current densities; (c) specific capacitance as a function of current densities; (d) Nyquist plots of EIS spectrum; (e) Ragone plot; (f) cycling stability at a current density of 0.5 A g^{-1} for 10,000 cycles.

yields sufficient surface area which can adsorb more electrolyte ions, resulting in a large capacitance; and (3) more mesopores in the porous structure are easier for electrolyte ion transport and adsorption that improves rate capacity and assists in ion diffusion to the bulk of the electrode that easily achieves access to the micropores [18,36–38].

4. Conclusions

In summary, we employed coconut fibers as the carbon source to prepare 3-dimensional HPAC via KOH activation. By adjusting the KOH/CFC mass ratio, the pore size distribution and the mesopore/micropore ratio were easily tuned and produced an interconnected amorphous texture. In the symmetric supercapacitor, the HPAC-4 material delivers large specific capacitance (266 F g^{-1} at 0.1 A g^{-1} in KOH electrolyte and 155 F g^{-1} at 0.1 A g^{-1} in $EMIMBE_4$ electrolyte), outstanding rate performance (maintaining 76% capacitance at 100 A g^{-1}) and enhanced cycling stability. Furthermore, the unique characteristics of multi-tubular hollow structure with hierarchical porosity, high specific surface area, and adequate electrical conductivity are all beneficial for high electrochemical performance, as the unique multi-tubular hollow structure with hierarchical porosity on the wall may effectively shorten the route for fast ion and electronic transport. Therefore, HPAC-4 shows promising electrode material for supercapacitor-based devices that combine high power (53 Wh kg^{-1}) with high energy density (8224 W kg^{-1}). These findings illustrated that the coconut fibers-based HPAC-4 material prepared through a cost-effective and facile method is promising for high-power and renewable energy storage devices.

Acknowledgment

This work was financially supported by the National Natural Science Foundation of China (Grant no. 51362009 and Grant no. 51162006), Key

Science & Technology project (ZDXM2015118) and International Science & Technology Cooperation program of Hainan (KJHZ2015-02).

References

[1] G. Wang, L. Zhang, J. Zhang, A review of electrode materials for electrochemical supercapacitors, Chem. Soc. Rev. 41 (2012) 797–828.
[2] X. Li, B. Wei, Supercapacitors based on nanostructured carbon, Nano Energy 2 (2013) 159–173.
[3] J. Yang, C. Zeng, F. Wei, J. Jiang, K. Chen, S. Lu, Cobalt–carbon derived from zeolitic imidazolate framework on Ni foam as high-performance supercapacitor electrode material, Mater. Des. 83 (2015) 552–556.
[4] M. Härmas, T. Thomberg, H. Kurig, T. Romann, A. Jänes, E. Lust, Microporous–mesoporous carbons for energy storage synthesized by activation of carbonaceous material by zinc chloride, potassium hydroxide or mixture of them, J. Power Sources (2016), http://dx.doi.org/10.1016/j.jpowsour.2016.04.038.
[5] S. Kandalkar, D. Dhawale, C.K. Kim, C. Lokhande, Chemical synthesis of cobalt oxide thin film electrode for supercapacitor application, Synth. Met. 160 (2010) 1299–1302.
[6] L.L. Zhang, X. Zhao, Carbon-based materials as supercapacitor electrodes, Chem. Soc. Rev. 38 (2009) 2520–2531.
[7] R.R. Salunkhe, Y. Kamachi, N.L. Torad, S.M. Hwang, Z. Sun, S.X. Dou, et al., Fabrication of symmetric supercapacitors based on MOF-derived nanoporous carbons, J. Mater. Chem. A 2 (2014) 19848–19854.
[8] Z. Jin, X. Yan, Y. Yu, G. Zhao, Sustainable activated carbon fibers from liquefied wood with controllable porosity for high-performance supercapacitors, J. Mater. Chem. A 2 (2014) 11706–11715.
[9] T. Tooming, T. Thomberg, H. Kurig, A. Jänes, E. Lust, High power density supercapacitors based on the carbon dioxide activated D-glucose derived carbon electrodes and 1-ethyl-3-methylimidazolium tetrafluoroborate ionic liquid, J. Power Sources 280 (2015) 667–677.
[10] H. Teng, C.T. Hsieh, Influence of surface characteristics on liquid-phase adsorption of phenol by activated carbons prepared from bituminous coal, Ind. Eng. Chem. Res. 37 (1998) 3618–3624.
[11] F.C. Wu, R.L. Tseng, C.C. Hu, C.C. Wang, Physical and electrochemical characterization of activated carbons prepared from firwoods for supercapacitors, J. Power Sources 138 (2004) 351–359.
[12] J. Chmiola, G. Yushin, Y. Gogotsi, C. Portet, P. Simon, P.L. Taberna, Anomalous increase in carbon capacitance at pore sizes less than 1 nanometer, Science 313 (2006) 1760–1763.
[13] H. Teng, Y.J. Chang, C.T. Hsieh, Performance of electric double-layer capacitors using carbons prepared from phenol–formaldehyde resins by KOH etching, Carbon 39 (2001) 1981–1987.
[14] D.D. Zhou, Y.J. Du, Y.F. Song, Y.G. Wang, C.X. Wang, Y.Y. Xia, Ordered hierarchical mesoporous/microporous carbon with optimized pore structure for supercapacitors, J. Mater. Chem. A 1 (2013) 1192–1200.
[15] M.Y. Ghotbi, M. Azadfalah, Design of a layered nanoreactor to produce nitrogen doped carbon nanosheets as highly efficient material for supercapacitors, Mater. Des. 89 (2015) 708–714.
[16] K. Xia, Q. Gao, J. Jiang, J. Hu, Hierarchical porous carbons with controlled micropores and mesopores for supercapacitor electrode materials, Carbon 46 (2008) 1718–1726.
[17] W.Y. Tsai, P.C. Gao, B. Daffos, P.L. Taberna, C.R. Pérez, Y. Gogotsi, et al., Ordered mesoporous silicon carbide-derived carbon for high-power supercapacitors, Electrochem. Commun. 34 (2013) 109–112.
[18] Z.S. Wu, Y. Sun, Y.Z. Tan, S. Yang, X. Feng, K. Müllen, Three-dimensional graphene-based macro-and mesoporous frameworks for high-performance electrochemical capacitive energy storage, J. Am. Chem. Soc. 134 (2012) 19532–19535.
[19] H. Wang, H. Yi, C. Zhu, X. Wang, H.J. Fan, Functionalized highly porous graphitic carbon fibers for high-rate supercapacitive electrodes, Nano Energy 13 (2015) 658–669.
[20] L. Chen, Y. Zhang, C. Lin, W. Yang, Y. Meng, Y. Guo, et al., Hierarchically porous nitrogen-rich carbon derived from wheat straw as an ultra-high-rate anode for lithium ion batteries, J. Mater. Chem. A 2 (2014) 9684–9690.
[21] M. Kunowsky, A. Garcia-Gomez, V. Barranco, J.M. Rojo, J. Ibáñez, J.D. Carruthers, et al., Dense carbon monoliths for supercapacitors with outstanding volumetric capacitances, Carbon 68 (2014) 553–562.
[22] W. Gu, M. Sevilla, A. Magasinski, A.B. Fuertes, G. Yushin, Sulfur-containing activated carbons with greatly reduced content of bottle neck pores for double-layer capacitors: a case study for pseudocapacitance detection, Energy Environ. Sci. 6 (2013) 2465–2476.
[23] C. Ma, Y. Song, J. Shi, D. Zhang, X. Zhai, M. Zhong, et al., Preparation and one-step activation of microporous carbon nanofibers for use as supercapacitor electrodes, Carbon 51 (2013) 290–300.
[24] W. Tian, Q. Gao, Y. Tan, K. Yang, L. Zhu, C. Yang, et al., Bio-inspired beehive-like hierarchical nanoporous carbon derived from bamboo-based industrial by-product as a high performance supercapacitor electrode material, J. Mater. Chem. A 3 (2015) 5656–5664.
[25] T.E. Rufford, D. Hulicova-Jurcakova, K. Khosla, Z. Zhu, G.Q. Lu, Microstructure and electrochemical double-layer capacitance of carbon electrodes prepared by zinc chloride activation of sugar cane bagasse, J. Power Sources 195 (2010) 912–918.
[26] T.E. Rufford, D. Hulicova-Jurcakova, Z. Zhu, G.Q. Lu, Nanoporous carbon electrode from waste coffee beans for high performance supercapacitors, Electrochem. Commun. 10 (2008) 1594–1597.
[27] X. Zhao, C. Johnston, P.S. Grant, A novel hybrid supercapacitor with a carbon nanotube cathode and an iron oxide/carbon nanotube composite anode, J. Mater. Chem. 19 (2009) 8755–8760.
[28] E. Ra, E. Raymundo-Piñero, Y. Lee, F. Béguin, High power supercapacitors using polyacrylonitrile-based carbon nanofiber paper, Carbon 47 (2009) 2984–2992.
[29] S.Y. Yang, K.H. Chang, H.W. Tien, Y.F. Lee, S.M. Li, Y.S. Wang, et al., Design and tailoring of a hierarchical graphene-carbon nanotube architecture for supercapacitors, J. Mater. Chem. 21 (2011) 2374–2380.
[30] P. Simon, Y. Gogotsi, Capacitive energy storage in nanostructured carbon–electrolyte systems, Acc. Chem. Res. 46 (2012) 1094–1103.
[31] M. Sevilla, R. Mokaya, Energy storage applications of activated carbons: supercapacitors and hydrogen storage, Energy Environ. Sci. 7 (2014) 1250–1280.
[32] Y. Korenblit, M. Rose, E. Kockrick, L. Borchardt, A. Kvit, S. Kaskel, et al., High-rate electrochemical capacitors based on ordered mesoporous silicon carbide-derived carbon, ACS Nano 4 (2010) 1337–1344.
[33] J. Hou, C. Cao, X. Ma, F. Idrees, B. Xu, X. Hao, et al., From rice bran to high energy density supercapacitors: a new route to control porous structure of 3D carbon, Sci. Rep. 4 (2014) 7260.
[34] D. Wang, G. Fang, T. Xue, J. Ma, G. Geng, A melt route for the synthesis of activated carbon derived from carton box for high performance symmetric supercapacitor applications, J. Power Sources 307 (2016) 401–409.
[35] W. Qian, F. Sun, Y. Xu, L. Qiu, C. Liu, S. Wang, et al., Human hair-derived carbon flakes for electrochemical supercapacitors, Energy Environ. Sci. 7 (2014) 379–386.
[36] D.W. Wang, F. Li, M. Liu, G.Q. Lu, H.M. Cheng, 3D aperiodic hierarchical porous graphitic carbon material for high-rate electrochemical capacitive energy storage, Angew. Chem. Int. Ed. 120 (2008) 379–382.
[37] Y. Li, Z. Li, P.K. Shen, Simultaneous formation of ultrahigh surface area and three-dimensional hierarchical porous graphene-like networks for fast and highly stable supercapacitors, Adv. Mater. 25 (2013) 2474–2480.
[38] S. Dutta, A. Bhaumik, K.C.W. Wu, Hierarchically porous carbon derived from polymers and biomass: effect of interconnected pores on energy applications, Energy Environ. Sci. 7 (2014) 3574–3592.